HEALTH AND MEDICINE

Precise closure of single blood vessels via multiphoton absorption–based photothermolysis

Yimei Huang[1,2,3]*, Zhenguo Wu[1,2]*, Harvey Lui[1,2], Jianhua Zhao[1,2], Shusen Xie[3], Haishan Zeng[1,2]†

We report a novel approach to selectively close single blood vessels within tissue using multiphoton absorption–based photothermolysis (multiphoton photothermolysis) without the need of exogenous agents. The treatment process is monitored by in vivo reflectance confocal microscopy in real time. Closure of single targeted vessels of varying sizes ranging from capillaries to venules was demonstrated. We also demonstrated that deeply situated blood vessels could be closed precisely while preserving adjacent overlying superficial blood vessels. In vivo confocal Raman spectroscopy of the treatment sites confirmed vessel closure as being mediated by local coagulative damage. Partial vessel occlusion could be achieved, and it is accompanied by increased intravascular blood cell speed. Multiphoton photothermolysis under real-time reflectance confocal imaging guidance provides a novel precision medicine approach for noninvasive, precise microsurgery treatment of vascular diseases on a per-vessel/per-lesion basis. The method could also be used for building ischemic stroke models for basic biology study.

INTRODUCTION

Forming one of the largest networks in our body, blood vessels deliver nutrients and oxygen to cells while also transporting their metabolic waste products for eventual elimination (*1*). Dysregulated blood vessels are found in a variety of clinical disorders involving neoplasia, dysmorphogenesis, or senescence. For example, cancer, capillary malformations (e.g., port wine stains), macular degeneration, and diabetic retinopathy are characterized or caused by excessive angiogenesis (*1*–*3*). Alternatively, insufficient vascular perfusion may cause organ ischemia or neurodegeneration (*1*).

Laser therapy has been widely used for treating hyperangiogenesis, such as occurs with macular degeneration (*4*), diabetic retinopathy (*5*), port wine stains (*6*–*10*), and cancer (*11*–*15*). Conventional laser therapy of pathologic vasculature is largely based on the principle of selective photothermolysis, wherein laser energy can be physically confined within targeted tissue by matching the appropriate wavelength and pulse duration according to a specific chromophore and tissue target (*6*, *16*). The visible-range absorption bands of hemoglobin (i.e., 415 to 430 nm and 542 to 577 nm) provide the basis for targeting blood vessels with lasers (*17*). Although the absorption coefficient in the 415- to 430-nm band is an order of magnitude higher than that of the 542- to 577-nm band, laser wavelengths within the latter band are usually used to maximize the differential absorption between hemoglobin and surrounding chromophores such as melanin and also to achieve deeper light penetration. The pulse duration of the laser should be shorter than the blood vessel thermal relaxation time to confine the laser-induced heat to the targeted blood vessels themselves, and at the capillary level, thermal relaxation times are within the millisecond domain (*16*). This now conventional, single-photon absorption approach to targeted laser therapy can be referred to as chromophore selective photothermolysis (CSP).

There are two limitations for CSP that could affect certain clinical applications. For blood vessels, the depth of the clinical effect is limited by the fact that the wavelengths used for optimal hemoglobin absorption fall short of the 650- to 950-nm "optical window" for tissue. The other challenge is that, with CSP, there is a potential for all blood vessels within the irradiated volume to be indiscriminately denatured, thereby impairing normal physiologic function after the disease is healed. Recently, researches have started to address the second limitation. For example, phantom experiments using laser pulses at eight different wavelengths between 585 and 1064 nm were explored to target deoxyhemoglobin to spare the arterial vessels (*18*).

We hereby introduce an anti-vascular treatment approach for achieving photothermolysis using multiphoton absorption to selectively close targeted single blood vessels without affecting other vessels and surrounding tissues. A tightly focused near-infrared (NIR) femtosecond (fs) laser beam is used to achieve instantaneously super-high power density ($>10^9$ W/cm^2) at the focal point to induce multiphoton absorption. This absorption is also restricted to the focal point only because, outside of this site, the power density is low. In preliminary work, we have demonstrated multiphoton absorption–based photothermolysis through experiments with ex vivo tissue samples (*19*, *20*). We refer to this approach as spatially selective photothermolysis (SSP) to distinguish it from the conventional single-photon absorption–based CSP. Because single-photon absorption is low within the tissue optical window, radiant energy can be efficiently directed to the target of interest by spatially aligning the laser focal point with the target. The focused laser beam will generate efficient multiphoton absorption at the target because the equivalent light absorption wavelength (i.e., incident wavelength/2) lies within the ultraviolet/deep blue range, where tissue/cellular components such as proteins and nucleic acids exhibit strong absorption. Outside of the focal point, there is no multiphoton absorption due to insufficient photon density, as well as no single-photon absorption due to the low tissue absorption coefficient in the NIR. In addition, NIR photons also penetrate more deeply than the visible wavelengths used with conventional single-photon absorption–based CSP.

[1]Imaging Unit, Integrative Oncology Department, BC Cancer Research Center, Vancouver, BC V5Z 1L3, Canada. [2]Photomedicine Institute, Department of Dermatology and Skin Science, University of British Columbia and Vancouver Coastal Health Research Institute, Vancouver, BC V5Z 4E8, Canada. [3]Key Laboratory of OptoElectronic Science and Technology for Medicine of Ministry of Education, Fujian Provincial Key Laboratory of Photonics Technology, College of Photonic and Electronic Engineering, Fujian Normal University, Fuzhou 350007, China.
*These authors contributed equally to this work.
†Corresponding author. Email: hzeng@bccrc.ca

In this work, we propose and demonstrate a novel approach for precisely targeted single blood vessel closure using multiphoton absorption–based SSP. Figure 1 illustrates the advantages of SSP over CSP for the proposed anti-vascular treatment. With this novel optical approach, it is possible to selectively close some vessels while leaving others intact to preserve normal tissue physiology once the disease is healed.

RESULTS

Imaging and closing blood vessel without exogenous agent

A multimodality optical system as shown in fig. S1 was developed and is capable of imaging, targeting, and closing a single blood vessel at a time in the mouse ear model. The system is also capable of measuring confocal Raman spectrum from a selected microlocation. A 785-nm continuous wave (cw) diode laser was used for reflectance confocal microscopy (cwRCM) to image and select target blood vessels for treatment. After treatment, cwRCM imaging was performed again to confirm blood vessel closure. The same cw laser is also used for confocal Raman measurements. A high-power Ti:sapphire fs laser tuned to 830-nm wavelength was used for blood vessel treatment. The laser beam was scanned over a small area inside a target vessel to perform the treatment. Reflectance confocal microscopy imaging based on the fs laser (fsRCM) was used to monitor the treatment procedure.

The blood vessel is easy to identify via RCM movie (movie S1). This is because the flowing blood cells cause large dynamic changes of the scattered optical signals detected by RCM. The flowing of the cells is readily visible in the movie. However, the contrast between the blood vessel and the surrounding tissue is low in single-frame images. It is difficult to determine whether the blood vessel has been closed according to the single-RCM image illustrated in Fig. 2A. To improve the contrast, we introduced an image processing algorithm, STD, which calculates the standard deviation of each pixel stack from 10 sequential frames of the RCM movie, as shown in Fig. 2B. Because blood cells flow in the vessel, the standard deviation of a pixel in the blood vessel is bigger than that in the surrounding tissues. Therefore, in the STD image, the blood vessel becomes bright, while the surrounding tissue becomes dark. This very well highlights the blood vessels in the image. To apply the STD algorithm, it is important to keep the measurement system stable. The STD images in Fig. 2C show that the "Y"-shaped blood vessel before treatment (top row) has changed to "V" shape (bottom row) after the closure of the vertical blood vessel, which is consistent with movies S1 and S2. Figure 2 (D to G) shows that blood vessels of different sizes were closed by adjusting the fs laser scanning irradiation area and the irradiation time.

Selective closure of blood vessel

One advantage of multiphoton photothermolysis is its capability of inducing highly spatially selective localized damage. We demonstrated that it can precisely occlude a targeted deeper blood vessel while preserving the overlying blood vessel, although the laser light traverses through it. Figure 3 shows such an example. There are two blood vessels in Fig. 3A. The vertical blood vessel marked with a white arrow is located under the other vessel marked with a red arrow. The orientation of the two blood vessels is illustrated in Fig. 3C. In the treatment, the laser beam was focused to the vertical blood vessel at the cross area to selectively close this vessel. Figure 3B shows that the vertical vessel blood flow disappears with the closure, while the other vessel above remains with blood flow. Movies S3 and S4 confirm the results shown in the STD images. Both movies S3 and S4 start at deeper depth and move toward the surface. A bright spot appears at the irradiation area in the RCM image when the blood vessel has been closed, as shown in Fig. 3D. The white spot might be due to the coagulation of blood cells.

Raman spectra of blood cells before and after blood vessel closure

To study the biochemical changes of the treatment site (white spot in Fig. 3D), we measured the Raman spectra of the site using the confocal Raman modality shown in fig. S1. We first compared the Raman spectra of blood cells and the surrounding tissue structures such as sebaceous gland and collagen to confirm the specificity of the blood cell Raman signal. The results are shown in fig. S2. The blood cell Raman spectrum is substantially different from the others. For instance, only the blood cell spectrum has the hemoglobin characteristic bands (418, 750, and 1543 cm^{-1}), while the sebaceous gland has the strongest fatty acid characteristic bands (1065, 1300, and 1442 cm^{-1}). We then measured the Raman spectra of blood cells before and after the blood vessel closure, as shown in Fig. 4. Table S1 lists the tentative Raman band assignment based on literature (*21*–*22*). The band at 377 cm^{-1}, the auto-oxidation marker, such as methemoglobin, greatly increased after treatment. The bending band of Fe-O_2, 418 cm^{-1}, decreased when the

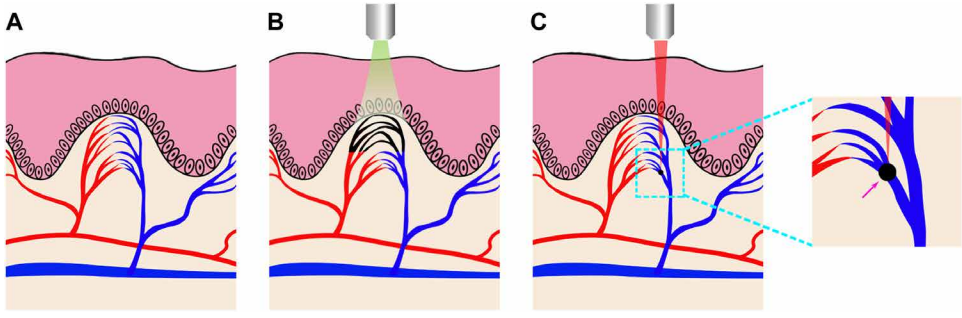

Fig. 1. Multiphoton absorption–based SSP versus conventional CSP for anti-vascular treatment within the skin. (**A**) Before exposure. (**B**) After conventional CSP, all vessels within the light irradiation volume are denatured (indicated by the black-colored blood vessels). (**C**) With SSP, the target vessel is denatured/closed because the tightly focused fs laser deposits the radiant energy in the target vessel (the focal point, indicated by the magenta arrow) through multiphoton absorption, a nonlinear optical phenomenon occurring only at the focal point with high enough light power density. Other vessels and surrounding tissues are not affected. The inset shows that the vessels above the target vessel are not altered, although the fs laser pulses pass through them. Comparing (B) with (C), SSP could also treat vessels located deeper, where CSP could not reach due to the limited penetration depth for visible light.

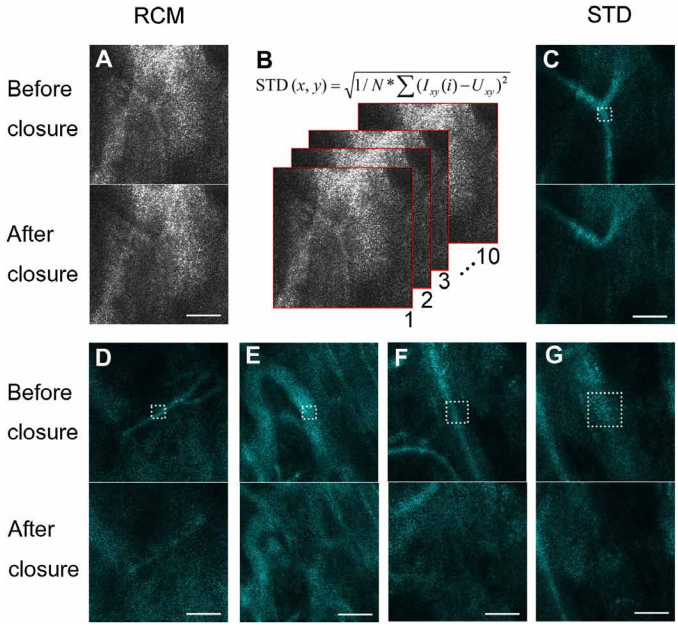

Fig. 2. Imaging blood vessel before and after closure. (**A** and **C**) RCM and STD images of the same blood vessel before and after closure. (**B**) Algorithm of STD. *N* is the frame number for calculation of STD (in this case, $N = 10$); $I_{xy}(i)$ is the pixel (x,y) intensity in the ith frame; U_{xy} is the average intensity at pixel (x,y) over all frames. (**D** to **G**) STD of different sized blood vessels before (top row) and after (bottom row) closure. The dashed white square boxes indicate the scanning irradiation area of the high-power treatment fs laser on the vessels. The pulse energy is 4.5 nJ per pulse, and the irradiation time is in the range of 0.1 to 2.1 s. Scale bars, 50 μm. (See movies S1 and S2 for more details.)

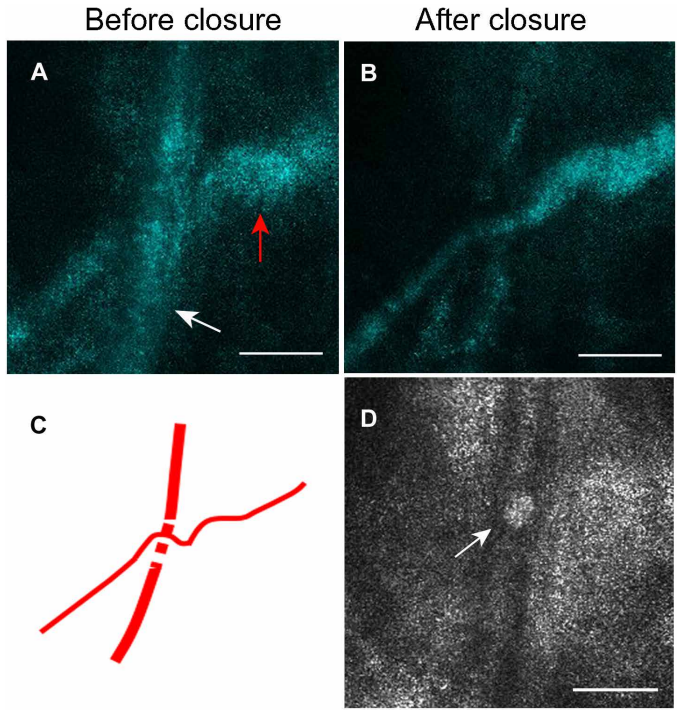

Fig. 3. Spatially selective blood vessel closure. (**A** and **B**) STD image of two blood vessels crossing over but located in different layers before (A) and after (B) treatment. The vertical blood vessel (white arrow) is at the bottom layer, and the other one (red arrow) is on the top layer. (**C**) Orientation of the two blood vessels. (**D**) RCM of the treated blood vessel at the bottom layer. The bright spot (white arrow) in (D) indicates the coagulation of blood cells. The laser pulse energy is 4.5 nJ per pulse, and the irradiation time is 4.5 s. Scale bars, 50 μm. (See movies S3 and S4 for more details.)

blood vessel was closed, indicating that the ligation between O_2 and Fe is weakened in the thermally induced heme aggregation. The vibration bands shifted from 677 and 754 cm^{-1} to 667 and 749 cm^{-1}, respectively, due to the denaturation of blood cells. The increasing intensities of the bands at 970 and 1248 cm^{-1} are attributed to the formation of hemoglobin and fibrin aggregates. All these band changes, including increase, decrease, and shift, could be attributed to the coagulation of blood cells.

Point treatment system

The results shown above were all obtained with the scanning system (fig. S1), which meant that the blood vessels were closed by scanning the high-power fs laser in the treatment area. Although the scanning system can monitor the fsRCM images during the high-power fs laser irradiation, the imaging field of view (FOV) is limited to the treatment area, and the effect of fs laser irradiation on the surrounding tissue cannot be monitored, as shown in movie S5. To overcome the limitations of the scanning system, we constructed a point treatment system, in which the fs laser beam does not pass through the scanner mirrors, as shown in fig. S3. The fs laser beam and the cw laser beam were combined with a dichroic mirror (DM) before the objective lens so that the switch between the two laser beams was not needed. The DM transmits 785-nm light and reflects 830-nm light. This point treatment system makes it possible to monitor the whole treatment process and evaluate the effect of blood vessel closure on the surrounding tissues.

Using the point treatment system, we studied the dynamics of blood flow during the high-power fs laser irradiation. Figure 5 is one of the typical examples. The red dashed lines in Fig. 5 (A to D) delineate the intraluminal margin of the blood vessel. The red dot in Fig. 5A indicates the fs laser irradiation position. The beam size is about 1 μm in the *X*-*Y* horizontal plane and 2 μm in the *Z* depth direction. A bright spot (Fig. 5B) appeared immediately after the high-power fs laser irradiated on the blood vessel. The bright spot evolved to a bright linear signal that aligned with the direction of blood flow (Fig. 5C) as the fs laser exposure continued. With increasing treatment time, the signal intensity at the focal point suddenly showed a marked increase, and the blood vessel began to contract, as shown in Fig. 5D. The whole treatment process appears in movie S6. We plotted the average image intensity over a 50 μm × 50 μm square around the focal point as a function of time (Fig. 5F), and it showed three events during the treatment. As the fs laser irradiated the blood vessel, the intensity increased greatly and lasted for about 1.5 s. With further laser exposure, the signal intensity increased even further to an even higher level (twofold). The signal intensity then decreased immediately when the vessel was closed and the fs laser was turned off.

Movie S6 shows interesting dynamics of the vessel closure process under point beam treatment. The associated physical, biochemical, and biological changes deserve further investigation, especially histological analysis.

Partial blood vessel occlusion

The point treatment system could be used to close a blood vessel completely. Furthermore, it could also be used to partially block a blood vessel, as shown in Fig. 6. We can see blood cells marked with red arrows

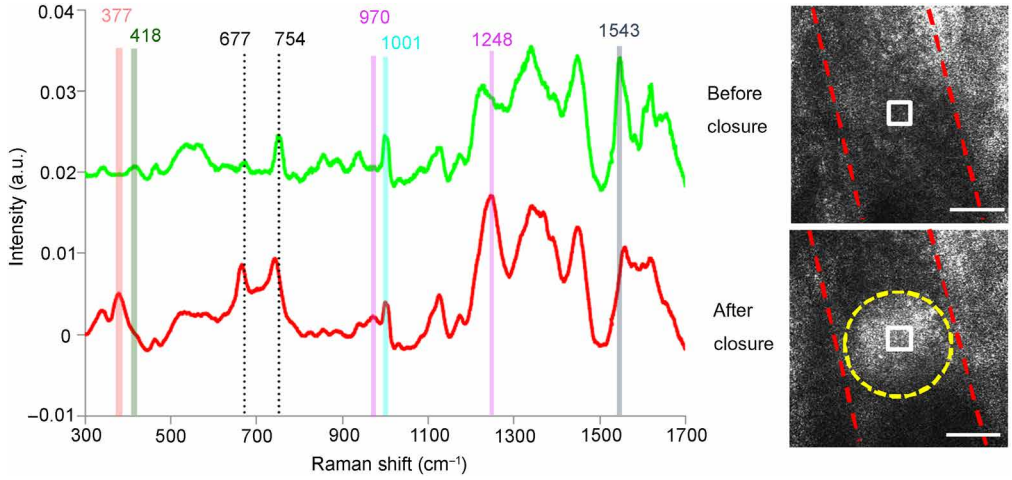

Fig. 4. Raman spectra of blood cells before (green curve) and after (red curve) the blood vessel closure. The Raman bands at 377 cm^{-1} (highlighted in vertical red line) and 970 and 1248 cm^{-1} (highlighted in magenta lines) increased, and the bands at 418 cm^{-1} (highlighted in dark green line) and 1543 cm^{-1} (highlighted in blue line) decreased. The bands at 677 and 754 cm^{-1} (black dashed lines) shifted to 667 and 749 cm^{-1}, respectively. The red dashed lines in the images indicate the blood vessel inner edges. The white square represents the fs laser treatment area. The yellow dashed circle indicates the coagulation region. Scale bars, 50 μm. a.u., arbitrary units.

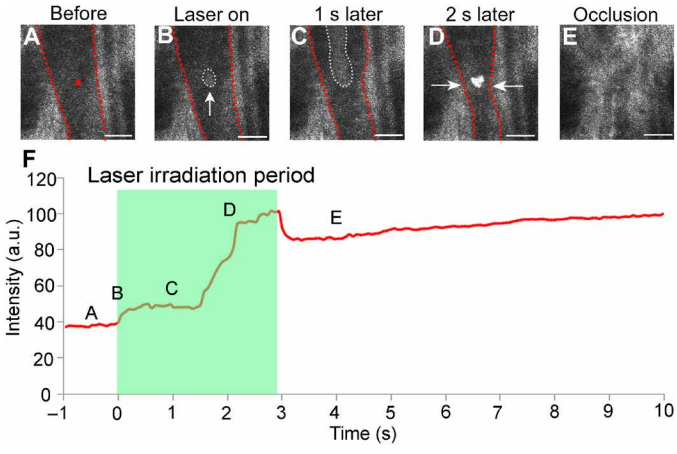

Fig. 5. Morphological dynamics of a large size blood vessel before, during, and after treatment using the point treatment system. (**A** to **E**) RCM images of the blood vessel before treatment, laser on, 1 s later, 2 s later, and after occlusion. The red dashed lines in (A) to (D) show the blood vessel edges. The red dot in (A) indicates the fs laser irradiation position. There is a bright spot [indicated by the arrow in (B)] at the fs laser irradiation position immediately after the laser is turned on. The bright spot becomes a bright stripe [as outlined by the white dashed curve in (C)] after the fs laser has irradiated for 1 s. A very bright spot appears after the fs laser has irradiated for 2 s, and the blood vessel begins to contract [as indicated by the arrow in (D)]. Scale bars, 50 μm (A to E). (**F**) Averaged intensity over an area surrounding the fs laser irradiation point (50 μm × 50 μm) variation with time. Time points (A) to (E) correspond to the images in panels (A) to (E), respectively. (See movie S6 for more details.)

before the laser irradiation (Fig. 6A). Both are bright spots. Some blood cells can also be visualized in the vessel after the laser irradiation (Fig. 6B), which indicates that the blood vessel has been partially blocked. The STD image (Fig. 6, C and D) and movie S7 also demonstrate that the blood vessel was partially blocked. The speed of blood cells could be calculated from the movie. We traced eight cells in the movie and calculated their speed before and after treatment. The results are shown in Fig. 6E. The mean speed of the eight cells increased by about 40%, from 0.021 to 0.029 mm/s, after partial closure of the vessel (Fig. 6E).

DISCUSSION

We developed two different systems for imaging the vessels, delivering the treatment fs laser beam, and monitoring the treatment process/effects. One system (fig. S1) enables the treatment beam to scan a region of interest (ROI) small area inside the vessel. Full field of view (FOV) RCM imaging is carried out before treatment to detect and select targeting vessel for closure. Full FOV image is taken again after treatment to assess the treatment effects. The treatment process can only be monitored by the ROI imaging, with the drawback of not seeing the surrounding tissues. The other system (fig. S3) enables point treatment (fs laser focal spot stays still) but full FOV monitoring of the therapy process. In our future studies, we will develop a more versatile system by adding another *X*-*Y* scanner between the fs laser and the DM in fig. S3 to realize variable ROI treatment under full FOV imaging guidance. This will enable us to design experiments to study whether there are differences between the point mode treatment and the ROI scanning mode treatment, as well as the effect of the ROI size on the treatment outcome. In both systems, the imaging beam and the treatment beam are well aligned with each other, and their focal planes are located accurately at the same depth level. The depth of treatment depends on the scattering properties of the tissue. The maximum depth could be about 400 μm for skin tissue and larger than 1 mm for brain tissue. For ophthalmology applications, we see no problem for the laser beam to penetrate through the eye ball and treat retinal blood vessels.

This study represents the first demonstration of multiphoton absorption–based photothermolysis (or simply called multiphoton photothermolysis) in vivo. We have demonstrated that precise closure of a single blood vessel can be achieved through multiphoton photothermolysis under RCM monitoring and without any need for an exogenous agent. Confocal Raman spectroscopy indicated that vessel closure was mediated by coagulation of blood cells. We also demonstrated that partial vessel occlusion could be achieved, and it is accompanied by increased intravascular blood cell speed.

Closing blood vessels with multiphoton photothermolysis could presumably be used to treat diseases related to excessive angiogenesis. The advantages of this approach over conventional (single-photon) photothermolysis treatment are more precise target selectivity and

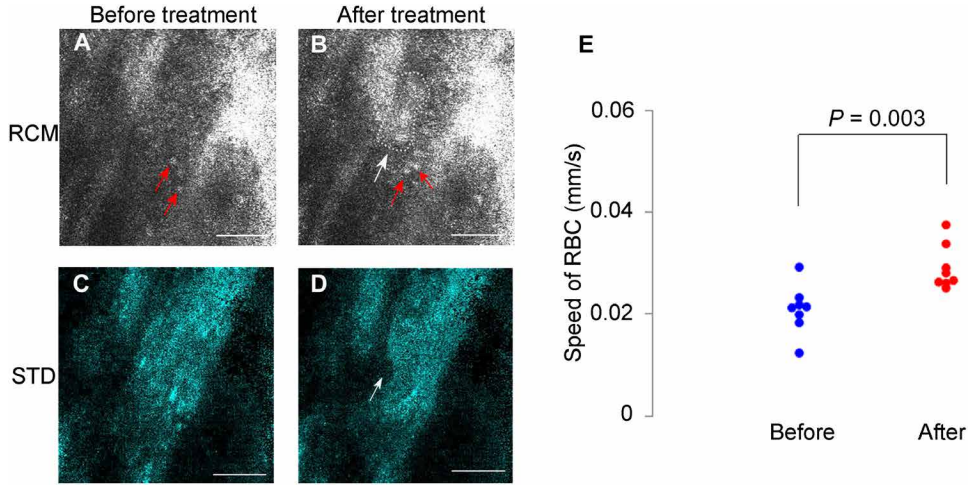

Fig. 6. Partial blood vessel occlusion. (**A** and **C**) RCM and STD images of a blood vessel before treatment. The blood cells marked with red arrows can be clearly identified. (**B** and **D**) RCM and STD images of the same blood vessel after treatment. Scale bars, 50 μm. The white arrow in (B) indicates the coagulation part, corresponding to the dark area in the STD image (D). The flowing cells indicated by red arrows in (B) suggest that the blood vessel was partially blocked. (**E**) Speed of red blood cells (RBCs) before and after treatment. The average speed of RBCs increased significantly, from 0.021 to 0.029 mm/s ($P < 0.05$, by paired t test; $n = 8$). (See movie S7 for more details.)

deeper effective treatment depth. Because this new technique is spatially selective, a single blood vessel could be closed precisely without damages to other neighbor vessels and surrounding tissues. This would allow selective denaturation of certain vessels while sparing other vessels to preserve normal tissue physiology once the disease is healed. Both the treatment and monitoring are label free and conducted in a noninvasive fashion. This is a precise "see and treat" microsurgery type anti-vascular method and holds particular promise for treating diseases in complex organs such as the eye (noninvasively) or brain, where high spatial selectivity is critical for preventing collateral effects on vision or central nervous system function. It represents a precision medicine approach for vascular disease treatment on a per-vessel/per-lesion basis.

Besides treatment of diseases related to excessive angiogenesis, closing blood vessels with multiphoton photothermolysis could also be used to create an ischemic stroke model. Stroke is one of the leading causes of death worldwide (*23*), and about 87% of stroke is of ischemic origin (*24*). Building ischemic stroke models would be of value to investigate the mechanism of ischemic stroke. Some technologies such as surgery ligation and drug administration have been used to build ischemic stroke model in murine animals (*25*–*28*). However, these technologies are not able to build precise ischemic stroke models. Nishimura *et al.* (*29*) have demonstrated that precise stroke models could be built with ultrashort laser pulses and injected fluorescein-conjugated dextran. However, the injected fluorescein-conjugated dextran may interact with the medicine when studying the effect of the medicine on ischemic stroke. The use of exogenous agent may also interfere with other biological processes; therefore, it is not desirable for basic vascular biology study. Conversely, in our approach, no exogenous agent is needed. This will benefit medicine investigation and basic vascular biology study.

MATERIALS AND METHODS

Study design

In this study, the in vivo targeting of single cutaneous vessels was demonstrated using a mouse ear model. In vivo RCM was used to localize a target vessel, monitor the treatment process, and then confirm the closure of the selected vessel. In vivo confocal Raman spectroscopy was used to characterize the biochemical changes at the targeted treatment sites for understanding the anti-vascular action mechanism.

Animal model

NODSCID mice were used in this study. In total, 83 blood vessels on the ears of 12 mice were treated with a fs laser beam. During laser treatment, the mice were anesthetized intraperitoneally with chloral hydrate (3%, 1 ml/100 mg). Mouse ear hair was removed with depilatory cream before laser treatment. The mouse ear for treatment was adhered to a glass slide with a double-sided tape. Distilled water was added in between the mouse ear and the microscope objective for refractive index matching. All animal experiments were performed according to a protocol approved by the University of British Columbia Animal Care Committee (certificate number: A10-0338).

Multimodality optical system for imaging and closure of blood vessel

A real-time (15 frames/s) multimodality optical microscopy system was developed to image and close blood vessels (fig. S1). A high-power Ti:sapphire fs laser (Chameleon, Coherent Inc., Santa Clara, CA) tuned to 830 nm was used for blood vessel treatment. The fs laser power on the mouse ear was 400 mW, which corresponded to 4.5 nJ per pulse with a 90-MHz pulse repetition rate. The total fs laser dose required to close a blood vessel varied with vessel diameter, blood cell speed, and the vessel depth within the skin. To control the fs laser fluence, the treatment procedure was monitored with fsRCM, in which the descanned fs laser reflectance signal was collected with an avalanched photodiode (APD). To avoid signal saturation and APD damage due to the intense fs laser power, the gain of the APD was reduced to the minimum, and one neutral density filter was used to attenuate the reflectance signal. A cw laser with a 785-nm wavelength was used to perform RCM imaging (cwRCM) before and after the fs laser treatment to confirm blood vessel closure. The cw laser was also used to excite the blood vessel Raman signal, which, in turn, was extracted with a DM. The DM reflects 785-nm light and transmits light at longer wavelengths.

A flip mirror was used to switch between these two lasers. The Raman spectrometer was equipped with a NIR-optimized back-illumination deep-depletion charge-coupled device (CCD) array (Spec-10:100BR/LN, Princeton Instruments, Trenton, NJ) and a transmissive imaging spectrograph (HoloSpec f/2.2 NIR, Kaiser, Ann Arbor, MI) with a volume phase technology holographic grating (HSG-785-LF, Kaiser). The CCD has a 16-bit dynamic range and was cooled with liquid nitrogen to −120°C.The spectral resolution of the system is 8 cm^{-1}.

Confocal Raman spectroscopy

The Raman spectra were collected and analyzed according to a similar approach in our previous work (*30*, *31*). In brief, with the confocal arrangement, the Raman signal was collected from the focal volume of the 785-nm cw laser beam. The excitation power incident on mouse ear was 20 mW, and the acquisition time for one spectrum was 20 s. The raw data included the Raman scattering and autofluorescence background. The autofluorescence background was removed using the Vancouver Raman Algorithm, which is based on an iterative polynomial fitting method (*32*).

Statistical analysis

Student's *t* test was used to evaluate the statistical difference. $P < 0.05$ means a significant difference.

SUPPLEMENTARY MATERIALS

Supplementary material for this article is available at http://advances.sciencemag.org/cgi/content/full/5/5/eaan9388/DC1

Fig. S1. Optical system for imaging and closing mouse ear blood vessels.
Fig. S2. In vivo confocal Raman spectra of blood cells, sebaceous gland, and collagen.
Fig. S3. Schematic of the point treatment system.
Table S1. Tentative assignment of Raman bands.
Movie S1. Y-shaped blood vessels before closure of the vertical blood vessel.
Movie S2. V-shaped blood vessel after closure of the vertical blood vessel.
Movie S3. Three-dimensional orientation of two blood vessels before treatment.
Movie S4. Three-dimensional orientation of two blood vessels after treatment.
Movie S5. fsRCM of the blood vessel during the fs laser treatment.
Movie S6. The dynamic process of the blood vessel closure using the point treatment system.
Movie S7. Partial closure of blood vessel.

REFERENCES AND NOTES

1. P. Carmeliet, Angiogenesis in health and disease. *Nat. Med.* **9**, 653–660 (2003).
2. J. Folkman, Role of angiogenesis in tumor growth and metastasis. *Semin. Oncol.* **29**, 15–18 (2002).
3. W. M. Al-zamil, S. A. Yassin, Recent developments in age-related macular degeneration: A review. *Clin. Interv. Aging* **12**, 1313–1330 (2017).
4. Macular Photocoagulation Study Group, Argon laser photocoagulation for neovascular maculopathy. Three-year results from randomized clinical trials. *Arch. Ophthalmol.* **104**, 694–701 (1986).
5. Early Treatment Diabetic Retinopathy Study Research Group, Treatment techniques and clinical guidelines for photocoagulation of diabetic macular edema: Early treatment diabetic retinopathy study report number 2. *Ophthalmology* **94**, 761–774 (1987).
6. R. R. Anderson, J. A. Parrish, Selective photothermolysis: Precise microsurgery by selective absorption of pulsed radiation. *Science* **220**, 524–527 (1983).
7. A. M. Chapas, K. Eickhorst, R. G. Geronemus, Efficacy of early treatment of facial port wine stains in newborns: A review of 49 cases. *Lasers Surg. Med.* **39**, 563–568 (2007).
8. L. Izikson, J. S. Nelson, R. R. Anderson, Treatment of hypertrophic and resistant port wine stains with a 755 nm laser: A case series of 20 patients. *Lasers Surg. Med.* **41**, 427–432 (2009).
9. S. W. Lanigan, S. M. Taibjee, Recent advances in laser treatment of port-wine stains. *Br. J. Dermatol.* **151**, 527–533 (2004).
10. Z. F. Jasim, J. M. Handley, Treatment of pulsed dye laser-resistant port wine stain birthmarks. *J. Am. Acad. Dermatol.* **57**, 677–682 (2007).
11. T. Soleymani, M. Abrouk, K. M. Kelly, An analysis of laser therapy for the treatment of nonmelanoma skin cancer. *Dermatol. Surg.* **43**, 615–624 (2017).
12. K. P. Allison, M. N. Kieman, R. A. Waters, R. M. Clement, Pulsed dye laser treatment of superficial basal cell carcinoma: Realistic or not? *Lasers Med. Sci.* **18**, 125–126 (2003).
13. P. Campolmi, L. Mavilia, P. Bonan, G. Cannarozzo, T. M. Lotti, 595 nm pulsed dye laser for the treatment of superficial basal cell carcinoma. *Lasers Med. Sci.* **20**, 147–148 (2005).
14. S. M. Shah, N. Konnikov, L. M. Duncan, Z. S. Tannous, The effect of 595 nm pulsed dye laser on superficial and nodular basal cell carcinomas. *Lasers Surg. Med.* **41**, 417–422 (2009).
15. N. Konnikov, M. Avram, A. Jarell, Z. Tannous, Pulsed dye laser as a novel non-surgical treatment for basal cell carcinomas: Response and follow up 12-21 months after treatment. *Lasers Surg. Med.* **43**, 72–78 (2011).
16. R. R. Anderson, Lasers for dermatology and skin biology. *J. Invest. Dermatol.* **133**, E21–E23 (2013).
17. R. Anderson, J. Parrish, in *The Science of Photomedicine*, J. D. Regan Ed. (Springer, 1982), pp. 147–194.
18. I. K. Rubin, W. A. Farinelli, A. Doukas, R. R. Anderson, Optimal wavelengths for vein-selective photothermolysis. *Lasers Surg. Med.* **44**, 152–157 (2012).
19. H. Wang, S. Zandi, A. M. Lee, J. Zhao, H. Lui, D. I. McLean, H. Zeng, Imaging directed photothermolysis through two-photon absorption demonstrated on mouse skin–a potential novel tool for highly targeted skin treatment. *J. Biophotonics* **7**, 534–541 (2014).
20. Y. Huang, H. Lui, J. Zhao, Z. Wu, H. Zeng, Precise spatially selective photothermolysis using modulated femtosecond lasers and real-time multimodal microscopy monitoring. *Theranostics* **7**, 513–522 (2017).
21. P. Lemler, W. R. Premasiri, A. DelMonaco, L. D. Ziegler, NIR Raman spectra of whole human blood: Effects of laser-induced and in vitro hemoglobin denaturation. *Anal. Bioanal. Chem.* **406**, 193–200 (2014).
22. Z. Movasaghi, S. Rehman, I. U. Rehman, Raman spectroscopy of biological tissues. *Appl. Spectrosc. Rev.* **42**, 493–541 (2007).
23. S.-Y. Li, D. Yang, Z. J. Fu, T. Woo, D. Wong, A. C. Y. Lo, Lutein enhances survival and reduces neuronal damage in a mouse model of ischemic stroke. *Neurobiol. Dis.* **45**, 624–632 (2012).
24. E. J. Su, D. A. Lawrence, α2 antiplasmin and microvascular thrombosis in ischemic stroke. *Arterioscler. Thromb. Vasc. Biol.* **34**, 2522–2523 (2014).
25. A. Selvamani, P. Sathyan, R. C. Miranda, F. Sohrabji, An antagomir to MicroRNA Let7f promotes neuroprotection in an ischemic stroke model. *PLOS ONE* **7**, e32662 (2012).
26. F. Bohmann, A. Mirceska, J. Pfeilschifter, E. Lindhoff-Last, H. Steinmetz, C. Foerch, W. Pfeilschifter, No influence of dabigatran anticoagulation on hemorrhagic transformation in an experimental model of ischemic stroke. *PLOS ONE* **7**, e40804 (2012).
27. K. Saita, M. Chen, N. J. Spratt, M. J. Porritt, G. T. Liberatore, S. J. Read, C. R. Levi, G. A. Donnan, U. Ackermann, H. J. Tochon-Danguy, J. I. Sachinidis, D. W. Howells, Imaging the ischemic penumbra with ^{18}f-fluoromisonidazole in a rat model of ischemic stroke. *Stroke* **35**, 975–980 (2004).
28. M. Daffertshofer, Z. Huang, M. Fatar, M. Popolo, H. Schroeck, W. Kuschinsky, M. A. Moskowitz, M. G. Hennerici, Efficacy of sonothrombolysis in a rat model of embolic ischemic stroke. *Neurosci. Lett.* **361**, 115–119 (2004).
29. N. Nishimura, C. B. Schaffer, B. Friedman, P. S. Tsai, P. D. Lyden, D. Kleinfeld, Targeted insult to subsurface cortical blood vessels using ultrashort laser pulses: Three models of stroke. *Nat. Methods* **3**, 99–108 (2006).
30. H. Wang, N. Huang, J. Zhao, H. Lui, M. Korbelik, H. Zeng, Depth-resolved in vivo micro-Raman spectroscopy of a murine skin tumor model reveals cancer-specific spectral biomarkers. *J. Raman Spectrosc.* **42**, 160–166 (2011).
31. H. Wang, A. M. D. Lee, H. Lui, D. I. McLean, H. Zeng, A Method for accurate in vivo micro-Raman spectroscopic measurements under guidance of advanced microscopy imaging. *Sci. Rep.* **3**, 1890 (2013).
32. J. Zhao, H. Lui, D. I. Mclean, H. Zeng, Automated autofluorescence background subtraction algorithm for biomedical Raman spectroscopy. *Appl. Spectrosc.* **61**, 1225–1232 (2017).

Acknowledgments: We appreciate the fruitful discussions with D. I. McLean during the course of the project. **Funding:** This work was supported by the Canadian Institutes of Health Research (grant MOP130548), the National Key Basic Research Program of China (grant 2015CB352006), the National Natural Science Foundation of China (61335011), the Canadian Dermatology Foundation, the VGH & UBC Hospital Foundation, and the BC Hydro Employees Community Services Fund. **Author contributions:** All authors contributed to designing the experiments, analyzing the results, and writing the manuscript. H.Z., Y.H., and H.L. conceived the project. Y.H. and Z.W. performed all the experiments reported in this paper. **Competing interests:** H.Z. and H.L. are inventors on a U.S. patent related to this work filed by BC Cancer Agency (no. 9687152B2, issued on 27 June 2017). The BC Cancer Agency, H.Z., and H.L. will receive royalties from any commercialization of the patent. The authors declare no other competing interests. **Data and materials availability:** All data needed to evaluate the conclusions in the paper are present in the paper and/or the Supplementary Materials. Additional data related to this paper may be requested from the authors.

Submitted 7 December 2018
Accepted 2 April 2019
Published 15 May 2019
10.1126/sciadv.aan9388

Citation: Y. Huang, Z. Wu, H. Lui, J. Zhao, S. Xie, H. Zeng, Precise closure of single blood vessels via multiphoton absorption–based photothermolysis. *Sci. Adv.* **5**, eaan9388 (2019).

Science Advances

Precise closure of single blood vessels via multiphoton absorption–based photothermolysis

Yimei Huang, Zhenguo Wu, Harvey Lui, Jianhua Zhao, Shusen Xie and Haishan Zeng

Sci Adv **5** (5), eaan9388.
DOI: 10.1126/sciadv.aan9388